JACS
JOURNAL OF THE AMERICAN CHEMICAL SOCIETY

Article

A Soft Porous Crystal based upon Organic Cages that Exhibits Guest-Induced Breathing and Selective Gas Separation

Zhifang Wang, Nivedita Sikdar, Shi-Qiang Wang, Xia Li, Meihui Yu, Xian-He Bu, Ze Chang, Xiaolong Zou, Yao Chen, Peng Cheng, Kuang Yu, Michael J. Zaworotko, and Zhenjie Zhang

J. Am. Chem. Soc., **Just Accepted Manuscript** • Publication Date (Web): 22 May 2019

Just Accepted

is published by the American Chemical Society. 1155 Sixteenth Street N.W., Washington, DC 20036

A Soft Porous Crystal based upon Organic Cages that Exhibits Guest-Induced Breathing and Selective Gas Separation

Zhifang Wang,[1,8] Nivedita Sikdar,[2] Shi-Qiang Wang,[2] Xia Li,[1,8] Meihui Yu,[7] Xian-He Bu,[7] Ze Chang,[7] Xiaolong Zou,[3,6] Yao Chen,[4,5] Peng Cheng,[1,8] Kuang Yu,*[3] Michael J. Zaworotko*[2] and Zhenjie Zhang*[1,4,8]

[1] College of Chemistry, Nankai University, Tianjin, 300071, China.

[2] Department of Chemical Sciences, Bernal Institute, University of Limerick, Limerick V94T9PX, Republic of Ireland.

[3] Center of Environmental Science and New Energy Technology, Tsinghua-Berkeley Shenzhen Institute, Tsinghua University, Shenzhen, 518055, China.

[4] State Key Laboratory of Medicinal Chemical biology, Nankai University, Tianjin 300071, China.

[5] College of Pharmacy, Nankai University, Tianjin, 300071, China.

[6] Shenzhen Geim Graphene Center and Low-Dimensional Materials and Devices Laboratory, Tsinghua-Berkeley Shenzhen Institute (TBSI), Tsinghua University, Shenzhen 518055, China.

[7] School of Materials Science and Engineering, Nankai University, Tianjin, 300071, China.

[8] Key Laboratory of Advanced Energy Materials Chemistry (MOE), Nankai University, Tianjin 300071, China

Dedicated to the 100th anniversary of Nankai University

ABSTRACT: Soft porous crystals (SPCs) that exhibit stimuli-responsive dynamic sorption behavior are attracting interest for gas storage/separation applications. However, design and synthesis of SPCs is challenging. Herein, we report a new type of SPC based on a [2+3] imide-based organic cage (**NKPOC-1**) and find that it exhibits guest-induced breathing behavior. Various gases were found to induce activated **NKPOC-1** crystals to reversibly switch from a "closed" nonporous phase (***α***) to two porous "open" phases (***β*** and ***γ***). The net effect is gate-opening behavior induced by CO_2 and C3 hydrocarbons. Interestingly, **NKPOC-1-*α*** selectively adsorbs propyne over propylene and propane at ambient conditions. Thus, **NKPOC-1-*α*** has the potential to separate binary and ternary C3 hydrocarbon mixtures and performance was subsequently verified by fixed bed column breakthrough experiments. In addition, molecular dynamics calculations and *in situ* X-ray diffraction experiments indicate that the gate-opening effect is accompanied by reversible structural transformations. The adsorption energies from molecular dynamics simulations aid are consistent with the experimentally observed selective adsorption phenomena. The understanding gained from this study of **NKPOC-1** supports the further development of SPCs for applications in gas separation/storage since SPCs do not inherently suffer from the recyclability problems often encountered with rigid materials.

INTRODUCTION

Soft porous crystals (SPCs) as exemplified by third-generation metal-organic frameworks (MOFs) are attracting attention for their stimuli-responsive behavior that is accompanied by reversible structural transformations.[1,2] Structural dynamism offers potential for applications as diverse as selective gas adsorption and separation,[3] gas storage,[4,5] sensing,[6] smart materials[7] etc. Until now, SPCs have concentrated on flexible MOFs[8-11] which can undergo reversible phase transformation(s) in response to external stimuli such as host-guest interaction,[12] temperature[11] or pressure.[14] In general, flexible MOFs that exhibit guest-dependent dynamic sorption function through organic linkers and metal or metal clusters can contort their structural features and thereby exhibit high working capacity and/or highly selective adsorption for specific gas molecules.[15-21] However, flexible MOFs are typically limited by high cost, complex synthesis and low stability to multiple cycles of regeneration. Exploring new classes of SPCs that can address these limitations is the focus of this contribution.

Molecular crystals formed by organic molecules or metal complexes are also known to undergo guest-dependent dynamic sorption behavior[22-24] but as they do not usually exhibit intrinsic porosity until they are subjected to an appropriate stimulus, they are in some ways counter-intuitive. Prototypal examples of SPCs based upon molecular crystals include calixarenes and Werner complexes as first studied by the groups of Atwood[25] and Barrer,[26] respectively. In both situations, non-porous molecular compounds were observed to transform to host-

guest compounds upon exposure to selected gases and/or vapors. Other examples have been reported[27-30] but they remain generally understudied. SPCs based upon MOFs are distinct from molecular solids in the forces that control their crystal structures; the former utilize coordinate covalent bonds, the latter weaker forces such as hydrogen bonding or van der Waals interactions[30,31] Molecular crystals might therefore be expected to undergo the phase transformations required of SPCs with lower activation energies and less strain than flexible MOFs.[1] Such molecular crystals provide a distinct strategy to create a new generation of guest-responsive materials.[32]

Porous organic cages (POCs)[33-37] are a relatively recently introduced type of molecular crystals and are ideal candidates to serve as SPCs[1,38] because they can exhibit both intrinsic porosity and extrinsic porosity. Moreover, POCs possess distinctly different features from network materials (e.g. MOFs, zeolites) especially solubility in common solvents. They can also offer high chemical stability, low density and good processability allowing for ease of handling, recrystallization and thin film-fabrication. However, although POCs have been developed for over a decade,[39-45] their use to prepare SPCs that exhibit stimuli-responsive dynamic sorption behavior and reversible structural transformations is underexplored. We report herein the synthesis of a [2+3] imide-based organic cage **NKPOC-1** (**NKPOC** = Nankai Porous Organic Cage) which exhibits both intrinsic and extrinsic porosity in the solid state (Scheme 1). Specifically, upon exposure to various gas molecules, activated **NKPOC-1** crystals reversibly switch from a "closed" nonporous phase (***α***) to two types of porous "open" phases (***β*** and ***γ***). We address the relevance of these phenomena to gas separations and use molecular dynamics (MD) calculations and *in situ* adsorption/PXRD experiments to study the mechanism of the gate-opening sorption behavior of **NKPOC-1**.

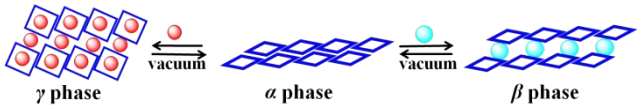

Scheme 1. The two structural transformations observed herein are likely to be general for POCs that form SPCs. For the ***α***→***β*** phase transformation, guest molecules (turquoise) reside between cages only; for the ***α***→***γ*** phase transformation, guest molecules (red) lie both within and between cages.

RESULTS AND DISCUSSION

Synthesis and characterization of **NKPOC-1**. **NKPOC-1** was prepared via a one-step condensation reaction of a flexible tri-amine and a rigid dianhydride in acetic acid (Figure 1a). The ^{1}H NMR spectrum (Figure S1) has three signals at 8.07, 7.47 and 6.35 ppm which can be assigned to hydrogen atoms on aromatic rings, indicative of the symmetric structure of **NKPOC-1.** Electrospray ionization mass spectrometry (ESI-MS) has a signal at *m/z* =1067.2991 corresponding to the expected [2+3] product $[C_{60}H_{42}N_8O_{12}]H^+$.

Rhombus-like single crystals of **NKPOC-1** were obtained through slow evaporation of **NKPOC-1** in dichloromethane and ethyl acetate. Single-crystal X-ray diffraction (SCXRD) revealed that **NKPOC-1** had crystallized in monoclinic *P*21/*c* (a = 20.7759 Å, b = 15.7504 Å, c = 18.2205 Å, β = 97.372°, V = 5913.0 Å^3) as a solvate, $C_{60}H_{42}N_8O_{12}$·*x*Solvent (**NKPOC-1-*β***, solvent = dichloromethane or ethyl acetate). As expected, **NKPOC-1** exists as a trigonal prismatic cage (Figure 1). The cage assembles into zigzag-shaped layers along the *bc* plane *via* π - π interactions between the benzofuran-1,3-dione rings (with a distance ~3.4 Å) (Figure 1b). Solvent molecules are located in cavities between the 2D layers (the interlayer distance measured between two nitrogen atoms in adjacent cages is ~7.9 Å, Figure 1c). No solvent was observed inside the cage. These results indicate that **NKPOC-1** is isolated as the ***β*** phase illustrated in Scheme 1. Powder X-ray diffraction (PXRD) confirmed bulk purity of the as-synthesized sample (Figure S2). Interestingly, *in-situ* PXRD revealed that **NKPOC-1-*β*** gradually loses solvent in air to form a new close-packed phase (**NKPOC-1-*α***), as indicated by shifting of PXRD peaks towards higher Bragg angles (Figure 1d).[46] The single crystal structure of **NKPOC-1-*α*** was obtained *via* slow drying of **NKPOC-1-*β*** in air and revealed that **NKPOC-1-*α*** is close-packed (Figure 1c) with a contracted (13.1%) unit cell (a =18.6187Å, b =15.7648 Å, c =17.9841 Å, β = 103.318 °, V =5136.7 Å^3). The 2D layers linked via π-π interactions are retained, while the interlayer distance is contracted from 7.9 to 5.6 Å. Additionally, we observed water molecules (one water molecule per cage determined by SCXRD) residing in a cavity between layers (Figure S3). In order to address the origin of the water molecules, we examined different drying conditions. Drying under vacuum at room temperature or at 120 ℃ both resulted in **NKPOC-1-*α*** as verified by PXRD (Figure S4). ^{1}H NMR spectra (Figure S5) further revealed that the water molecules observed in **NKPOC-1-*α*** were likely adsorbed from air since water was not detected under other drying conditions. These observations indicated to us that **NKPOC-1** could exhibit stimuli-responsive behavior and prompted us to study this matter further.

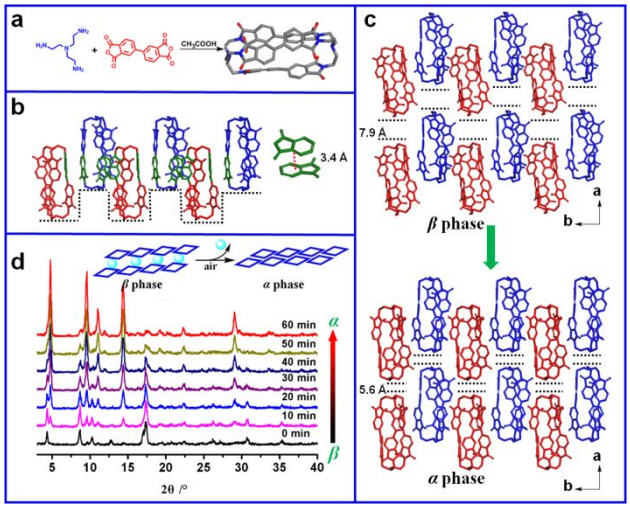

Figure 1. (a) Synthesis of **NKPOC-1** (C gray, N blue, O red). (b) Crystal structure of **NKPOC-1-*β*** viewed along the *c* axis and *ab* planes (left, collected at 120 K), respectively. (c) Crystallographic figures of the close-packing in **NKPOC-1-*α*** (bottom) and **NKPOC-1-*β*** phase (top) along *c* axis and *ab* plane. (d) Transformation of as-synthesized **NKPOC-1-*β*** to **NKPOC-1-*α*** in air monitored by PXRD.

Adsorption Experiments. N_2 sorption at 77 K revealed that activated **NKPOC-1-*α*** did not adsorb significant amounts of N_2 (Figure 2). CO_2 sorption at 195 K revealed that **NKPOC-1-*α*** exhibits multi-steps and hysteresis in the desorption isotherm. These results suggest structural flexibility of **NKPOC-1-*α***. In the first step, abrupt adsorption was observed at 1.8 kPa and CO_2 uptake rose to 58.0 cm^3/g by 11.7 kPa. In the second step, CO_2 uptake reached 76.2 cm^3/g at 22.2 kPa. The third step was from 22.2 to 45.0 kPa with CO_2 uptake of 137.0 cm^3/g. The last step proceeds gradually until saturation (165 cm^3/g at 100 kPa). These results suggest that activated **NKPOC-1-*α*** is nonporous to N_2 but undergoes phase changes induced by CO_2 at 195 K. High pressure sorption data for CO_2, N_2 and CH_4 collected at 298 K revealed CO_2 uptake of 83.9 cm^3/g at 44 bar and negligible N_2 (3.7 cm^3/g) and CH_4 (3.5 cm^3/g) uptake at 44 bar (Figure S6). Moreover, we found that after five consecutive cycles of low-pressure CO_2 sorption at 195 K or 100 cycles of high-pressure CO_2 sorption at 298 K, CO_2 uptakes and gate adsorption pressures were retained (Figure 2b and S7).

In order to gain insight into the structural changes of **NKPOC-1-*α*** upon CO_2 sorption, *in situ* adsorption coupled with PXRD was conducted under variable gas pressures at 195 K (Figure 2c). **NKPOC-1-*α*** did not transform to **NKPOC-1-*β*** at these conditions. Based on molecular dynamics simulations and other gas sorption data (see next section and the molecular dynamics section), we concluded that **NKPOC-1-*α*** undergoes multiple transformations before it reaches **NKPOC-1-*γ***, the phase in which CO_2 molecules are adsorbed both between and within the cages (Scheme 1). PXRD data revealed that **NKPOC-1-*γ*** reversibly reverts to **NKPOC-1-*α*** upon exposure to vacuum (Figure S7b).

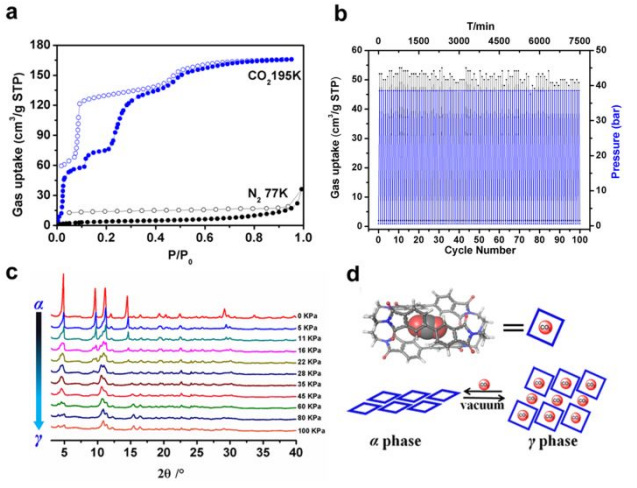

Figure 2. (a) Gas sorption isotherms of activated **NKPOC-1-*α*** at 77 K (N_2) and 195 K (CO_2). (b) Cyclability test of CO_2 adsorption at 298 K for crystalline **NKPOC-1-*α*** under high pressure. (c) In-situ X-ray powder diffraction patterns of activated **NKPOC-1-*α*** under variable gas pressures at 195 K indicate the possibility of a direct ***α*→*γ*** phase change. (d) A schematic illustration of the ***α*→*γ*** phase change.

The CO_2 breathing behavior of **NKPOC-1-*α*** prompted us to further study sorption properties with respect to other gases such as C3 hydrocarbons (propyne: C_3H_4, propylene: C_3H_6; propane: C_3H_8), which are important industrial feed stocks. The adsorption/desorption isotherms for C_3H_4, C_3H_6 and C_3H_8 were measured at 253 K (Figure 3a) and revealed a Type I isotherm for C_3H_4 with an uptake of 85.1 cm^3/g at 100 kPa. C_3H_6 and C_3H_8 exhibited gate-opening behavior (12.1 kPa for C_3H_6 and 30.2 kPa for C_3H_8) and adsorption-desorption hysteresis with almost the same uptake of 72.6 cm^3/g at 100 kPa. The gate-opening pressure was observed to increase with temperature. For example, at 273 K (Figure 3b), the gate-opening pressures for C_3H_4, C_3H_6 and C_3H_8 were found to be 3.5, 36.2, and 97.2 kPa, respectively. At 298 K or 318 K there was almost no uptake for C_3H_6 and C_3H_8, but high uptake for C_3H_4 was retained (> 80.0 cm^3/g, Figure 3c, 3d). Plotting the gate-opening pressure versus temperature for C_3H_4 (Figure S8) suggests an enthalpy of 37.5 kJ/mol for the gate opening.[47] Multi-cycle C_3H_4 adsorption-desorption isotherms were collected for **NKPOC-1-*α*** to investigate its recyclability at 273 K. The C_3H_4 uptake and gate opening pressure remained constant even after 8 cycles (Figure S9). In addition, FT-IR spectra of desolvated **NKPOC-1-*α*** exposed to C_3H_4 at 298 K demonstrated the characteristic stretching vibration of C_3H_4 at 3256 cm^{-1} (Figure S10), indicating that C_3H_4 is captured by **NKPOC-1-*α***. These results indicate potential utility of **NKPOC-1-*α*** for C3 hydrocarbon separations under ambient conditions.

In order to study structural changes on C3 hydrocarbon adsorption and directly observe guest-induced structural transformations, *in-situ* X-ray powder diffraction experiments were performed with C_3H_6 (C_3H_4 was not tested because it causes corrosion) under variable gas pressures at 253 K. The *in situ* PXRD data agreed well with the adsorption experiments (Figure 4a). Figure 4b reveals that no structural change occurs at 21 kPa or below. New diffraction peaks appeared from ~35 kPa, suggesting a structural change. The pristine **NKPOC-1-*α*** phase had completely disappeared by ~67 kPa and the PXRD pattern agreed well with that of **NKPOC-1-*β***. It was found that **NKPOC-1-*β*** readily transformed back to **NKPOC-1-*α*** after C_3H_6 desorption (Figure S11).

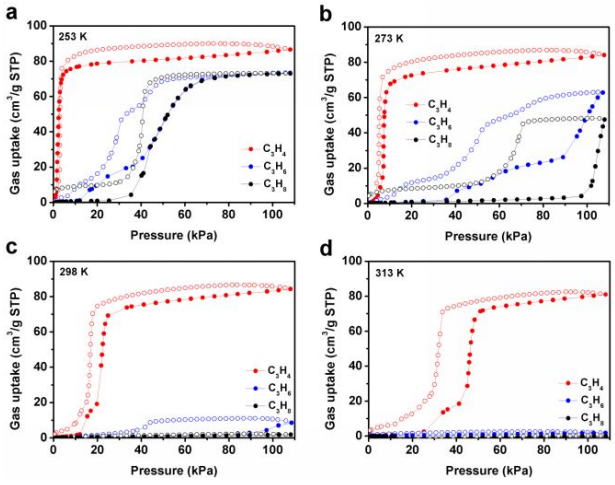

Figure 3. Sorption isotherms of **NKPOC-1-*α*** for C_3H_4, C_3H_6 and C_3H_8 at (a) 253 K, (b) 273 K, (c) 298 K, (d) 313 K. Filled and open symbols represent adsorption and desorption, respectively.

We next determined if sorbed gases reside inside or outside the cages by studying amorphous **NKPOC-1** obtained via a freeze-drying method (Figure S12 and S13). Amorphous samples adsorbed a relatively low amount of C_3H_4 (15.6 cm^3/g at 108 kPa) at 298 K (Figure S14), indicating that the gate-opening of **NKPOC-1-*α*** results from extrinsic porosity. This conclusion is further supported by molecular dynamic simulations as detailed in the following section. We also noted that grinding of samples had only a small effect upon kinetics and no effect upon uptake (Figure S8).

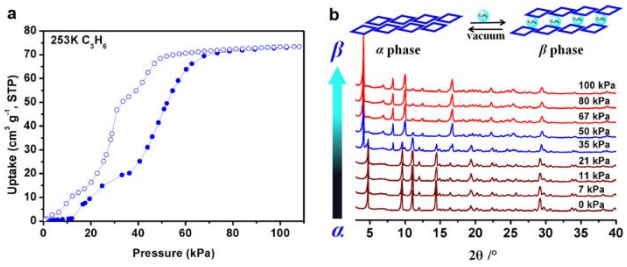

Figure 4. (a) Adsorption and desorption isotherms of activated **NKPOC-1-*α*** for C_3H_6 at 253 K. (b) In-situ PXRD experiments collected under variable gas pressures at 253 K.

Molecular Dynamics Simulations. To understand the nonporous-to-porous phase transformation process, we studied the microscopic adsorption mechanism of **NKPOC-1** using MD simulations (see numerical details in SI). We first computed the free energy profiles of CO_2, C_3H_4, and C_3H_6 intercalating inside a single **NKPOC-1** cage (C_3H_8 is not included as it is even more difficult to intercalate than C_3H_6, whose intercalation is already unfavored (vide infra)). The results are given in Figure S15 and S16. At 195 K, CO_2 features a strong binding site at the surface of the cage (rCOM = 7.5 Å) and a weaker binding site (rCOM = 0 Å). These two sites are separated by a 20 kJ/mol free energy barrier, and both are associated with favorable negative free energies. In contrast, at 298 K, both C3 molecules are unable to enter the cage, as indicated by the positive free energies at rCOM = 0. These results imply that the adsorption of CO_2 and C3 molecules may happen through different mechanisms, as we explain below.

In order to study the sorption-induced phase transitions in more detail, we performed simulations based upon the crystal structure of **NKPOC-1-*α***. MD simulation reproduces all the experimental lattice parameters of **NKPOC-1-*α*** within 3% except for the β angle (111° *vs.* 103°). Starting from this activated structure, we adopted a "greedy algorithm" (see details in SI) to determine the positions and energies of the adsorbed molecules. In the following discussion, we address the C3 gas results and then CO_2, which is more complicated.

For C3 gases, significant structural changes occurred when three molecules were loaded per cage. For C_3H_4, the *a* axis increased from 19.2 Å to 21.1 Å, and the β angle shrunk from 111° to 99°. Both changes agree with the experimental trends (the *a* axis increases from 18.7 Å to 20.8 Å, β decreases from 103° to 97°). All gas molecules reside in the extrinsic pores, and the experimental structure **NKPOC-1-*β*** was reproduced. In Figure 5c, we illustrate simulated **NKPOC-1-*β*** fully loaded with C_3H_4 (green shaded areas mark the cavities).

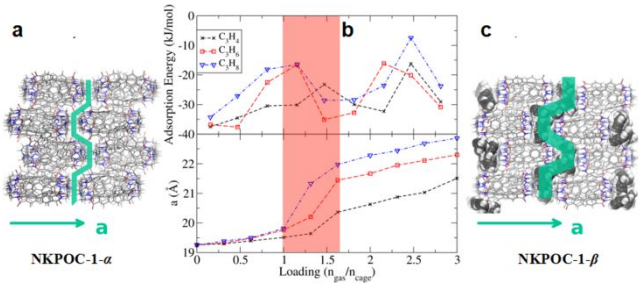

Figure 5. Crystal structures of **NKPOC-1** and their gas adsorption energies. a) The simulated crystal structure of activated **NKPOC-1-*α***; b) the adsorption energies at 298 K and the lattice parameter '*a*' plotted against the loading amount; c) the simulated crystal structure of fully loaded (n_{gas}/n_{cage}=3) **NKPOC-1-*β***.

The adsorption energies at different loading stages were computed using the following equation:

$$E_{ads}\left(N+\frac{\Delta N}{2}\right)=\frac{\left\langle E(N+\Delta N)\right\rangle-\left\langle E(N)\right\rangle-\Delta N\left\langle E_{gas}\right\rangle}{\Delta N}$$

Here, $\triangle N$ is the number of inserted molecules, E_{gas} is the total energy of a single gas molecule at the corresponding temperature, and <…> denotes the ensemble average over the MD trajectory. The resulting adsorption energies at 298 K are plotted in the upper panel of Figure 5b, with the lengths of *a* axis plotted in the lower panel, both as functions of loading ratio. Adsorption energies at a lower temperature (253 K) are also available in Figure S17. For all three C3 gas species, the *a* value drastically increases between a loading ratio of 1.0-1.5 (illustrated by the red shaded area), thereby forming cavities between POCs. This transition region happens at uptake of 21~32 cm^3/g, corresponding to 20 kPa–40 kPa of external pressure Figure 4a). This concurs with the results reported in Figure 4b, which reveal that the ***α*→*β*** transition happens between 21-67 kPa. Meanwhile, in the same region, the adsorption energy increases (unfavorable for adsorption) due to the energy penalty associated with cavity formation. After the cavities are created, more gas molecules can be adsorbed with more favorable adsorption energies until the voids are completely filled. Consequently, the adsorption energy features a wavy shape (see Figure 5b), fluctuating by ~20 kJ/mol. it is likely that such a wavy-shape will be carried over to the chemical potential profile, impacting its adsorption behavior in a profound way. We schematically illustrate the wavy chemical potential in Figure 6. During the adsorption process, the chemical potential (μ) increases with external pressure, and the system evolves following the blue path. When the system climbs to the spinodal point A, it leaps forward in loading capability, leading to the s-shape " switch-on " feature of the experimental isotherm. Meanwhile, during the desorption process, the system follows the red path, which also features a discontinuous "switch-off" at the spinodal point B. The two spinodal points A and B correspond to different μ, giving rise to the hysteresis. Quantitative chemical potential analysis is ongoing in our lab in order to further verify this assumption.

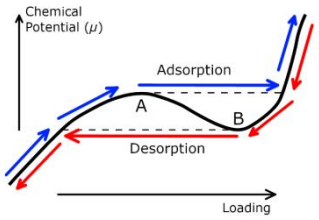

Figure 6. Schematic illustration of the adsorption/desorption process.

The on/off switching behavior observed herein can be advantageous for gas storage and separation applications as only a small change of pressure is required to promote adsorption/desorption. This is especially the case when the switching occurs between closed and open phases, as observed herein. The resulting S-shaped or "Type F-IV"[48] isotherms are quite distinct from the Langmuir or "Type I" isotherms typically seen for rigid porous materials. Importantly, such switching isotherms can maximize the selectivity of the adsorbent even when only small differences in adsorption energy are in play. By comparing the heights of the first peak of the adsorption energy (i.e., the activation energy of the "switch-on" process), we can predict the selectivity of **NKPOC-1-*α*** for gas molecules. According to Figure 5b, the order of the activation energy is $C_3H_8 \approx C_3H_6 < C_3H_4$, indicating facile switch-on for C_3H_4 vs. C_3H_8. These results are once again in agreement with experimental data. These simulation results, in combination with our experimental data presented above, suggest that **NKPOC-1-*α*** could be an effective adsorbent to separate C3 gases.

For CO_2, adsorption energy and *a* axis elongation results are presented in Figure S18 and S19. Consistent with experimental data, **NKPOC-1-*α*** possesses a high affinity for CO_2. The adsorption energy is -30 kJ/mol up to a loading ratio of 2 (42 cm^3/g uptake). The phase transition does not occur until 3.16 loading ratio (66 cm^3/g uptake), matching the experimental data in Figure 2a. Most interestingly, we observed CO_2 molecules entering the intrinsic pores in our simulations, which did not occur for C3 molecules. The resulting structure at 126 cm^3/g uptake is shown in Figure S20; both intrinsic and extrinsic sites are occupied. CO_2 is therefore predicted to adsorb in **NKPOC-1-α** and afford the ***γ*** phase (Scheme 1 and Figure 2d). That the modelling results indicate that both the intrinsic and extrinsic pores can be partially occupied with CO_2 molecules at all loadings suggests that it is possible for the ***γ*** phase to directly transform from the ***α*** phase through a "one-phase" mechanism, i.e. without forming a transient ***β*** phase, under certain conditions. Conversely, the room temperature high pressure recycling data is consistent with transformation between **NKPOC-1-α** and **NKPOC-1-*β***.

Experimental Gas Mixture Breakthrough. As shown in Figure 3c, the C_3H_4 uptakes for **NKPOC-1-*α*** are systematically higher than C_3H_6 and C_3H_8 at 298 K, suggesting propensity for C_3H_4/C_3H_6, C_3H_4/C_3H_8 and $C_3H_4/C_3H_6/C_3H_8$ separations. It is possible to use single-component adsorption isotherms to estimate the adsorption selectivity of porous materials. The ratio of C_3H_4/C_3H_6 and C_3H_4/C_3H_8 adsorbed at 90 kPa and 298 K are 29.3 and 51.2 respectively, indicating that **NKPOC-1-*α*** is potentially useful for separating C_3H_4 from C_3H_6 or C_3H_8 at near ambient temperature. To examine the separation performance, kinetically controlled real-time fixed-bed column breakthrough experiments were conducted using binary and ternary gas mixtures of C_3H_4/C_3H_6 (2:1, v/v) and C_3H_4/C_3H_8 (2:1, v/v) at 298 K (Figure 7a). **NKPOC-1-*α*** exhibited excellent separation performance towards C_3H_4 for the binary C_3H_4/C_3H_6 and C_3H_4/C_3H_8 gas mixtures with C_3H_4 saturation uptakes and breakthrough retention times of 75.6 cm^3/g, 137 min/g and 55.2 cm^3/g, 100 min/g, respectively. The C_3H_6 and C_3H_8 purity in the outlet gas streams were 98.5% and 98.0 % (Figure S21a), respectively. To further examine the potential of **NKPOC-1-*α*** for removal of C_3H_4 from a C_3H_6 and C_3H_8, a breakthrough experiment with a ternary gas mixture $C_3H_4/C_3H_6/C_3H_8$ (2:1:1, v/v/v) (Figure 7b) was conducted under ambient conditions. C_3H_4 was retained in the packed column for 135 min/g and the C_3H_4 saturation uptake was calculated to be 67 cm^3/g (Figure 7b and S21b). This good separation performance of **NKPOC-1-*α*** can be attributed to its selective gate-opening effect for C3 hydrocarbons and the strength of the interactions once open. Although the overall performance of **NKPOC-1-*α*** for C3 hydrocarbon separation does not surpass benchmark MOF materials,[49,50] we consider our study to be the first demonstration of the use of SPCs for C3 hydrocarbon separation. Compared with MOFs, the major advantages of **NKPOC-1-*α*** lie with high water stability (Figure S22), facile regeneration (Figure S23) and relatively low cost.

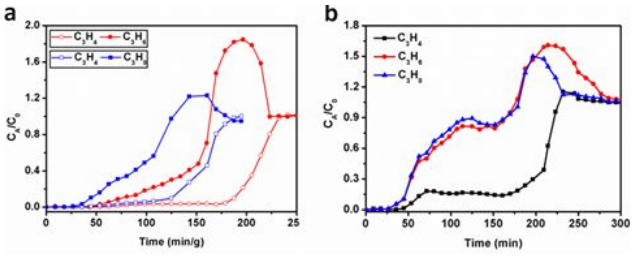

Figure 7. (a) Dynamic experimental fixed-bed column breakthrough results of binary (2:1, v/v) C_3H_4/C_3H_6 and C_3H_4/C_3H_8 gas mixtures in an absorber bed packed with activated **NKPOC-1-*α***; (b) ternary breakthrough experiment of $C_3H_4/C_3H_6/C_3H_8$ (2:1:1, v/v/v) gas mixture.

CONCLUSION

In this study we report a new type of soft porous crystals based on a new organic cage (**NKPOC-1**). **NKPOC-1** exhibits guest-induced breathing behavior with CO_2 and C3 hydrocarbons promoting activated **NKPOC-1** crystals to reversibly switch from a "closed" nonporous phase (***α***) to two porous "open" phases (***β*** or ***γ***). The adsorption-induced reversible structural transformations were studied via single crystal structure analysis, *in situ* adsorption/X-ray diffraction experiments and molecular dynamics simulations. **NKPOC-1-α** exhibits gate opening or abrupt adsorption for propyne but not for propylene and propane at ambient condition. This selective gate opening effect can explain why **NKPOC-1-α** can highly efficiently separate binary or ternary C3 gas mixtures as verified by fixed bed column breakthrough experiments. This report is the first demonstration of the potential to use molecular SPCs for C3 hydrocarbon separation. The

strategy of using organic cages to form SPCs is of broad scope and is likely to offer a new approach to utilizing molecular crystals for gas separations.

ASSOCIATED CONTENT

Supporting Information

The Supporting Information is available free of charge on the ACS Publications website.
Experimental procedures, simulation details, NMR data, PXRD, gas sorption data, extra figures, tables.

AUTHOR INFORMATION

Corresponding Author

*yu.kuang@sz.tsinghua.edu.cn

*Michael.Zaworotko@ul.ie

*zhangzhenjie@nankai.edu.cn

Author Contributions

The manuscript was written through contributions of all authors. All authors have given approval to the final version of the manuscript.

Notes

The authors declare no competing financial interests.

ACKNOWLEDGMENT

The authors acknowledge the financial support from the National Natural Science Foundation of China (21601093), Tianjin Natural Science Foundation of China (17JCZDJC37200) and Science Foundation Ireland (13/RP/B2549, 16/IA/4624).

REFERENCES

(1) Horike, S.; Shimomura, S.; Kitagawa, S. Soft porous crystals. *Nat. Chem.* **2009**, *1*, 695-704.

(2) Kitagawa, S.; Kondo, M. Functional Micropore Chemistry of Crystalline Metal Complex-Assembled Compounds. *Bull. Chem. Soc. Jap.* **1998**, *71* (8), 1739-1753.

(3) Li, J.-R.; Sculley, J.; Zhou, H.-C. Metal–Organic Frameworks for Separations. *Chem. Rev.* **2012**, *112* (2), 869-932.

(4) He, Y.; Zhou, W.; Qian, G.; Chen, B., Methane storage in metal-organic frameworks. *Chem. Soc. Rev.* **2014**, *43* (16), 5657-5678.

(5) Makal, T. A.; Li, J.-R.; Lu, W.; Zhou, H.-C., Methane storage in advanced porous materials. *Chem. Soc. Rev.* **2012**, *41* (23), 7761-7779.

(6) Kreno, L. E.; Leong, K.; Farha, O. K.; Allendorf, M.; Van Duyne, R. P.; Hupp, J. T. Metal–Organic Framework Materials as Chemical Sensors. *Chem. Rev.* **2012**, *112* (2), 1105-1125.

(7) Troyano, J.; Carné-Sánchez, A.; Pérez-Carvajal, J.; León-Reina, L.; Imaz, I.; Cabeza, A.; Maspoch, D. A Self-Folding Polymer Film Based on Swelling Metal–Organic Frameworks. *Angew. Chem. Int. Ed.* **2018**, *57* (47), 15420-15424.

(8) Lin, Z. J.; Lu, J.; Hong, M.; Cao, R. Metal-organic frameworks based on flexible ligands (FL-MOFs): structures and applications. *Chem. Soc. Rev.* **2014**, *43* (16), 5867-5895.

(9) Schneemann, A.; Bon, V.; Schwedler, I.; Senkovska, I.; Kaskel, S.; Fischer, R. A. Flexible metal-organic frameworks. *Chem. Soc. Rev.* **2014**, *43* (16), 6062-6096.

(10) Zhang, J. P.; Liao, P. Q.; Zhou, H. L.; Lin, R. B.; Chen, X. M. Single-crystal X-ray diffraction studies on structural transformations of porous coordination polymers. *Chem. Soc. Rev.* **2014**, *43* (16), 5789-5814.

(11) Alhamami, M.; Doan, H.; Cheng, C. H. A Review on Breathing Behaviors of Metal-Organic-Frameworks (MOFs) for Gas Adsorption. *Materials* **2014**, *7* (4), 3198-3250.

(12) Serre, C.; Mellot-Draznieks, C.; Surblé, S.; Audebrand, N.; Filinchuk, Y.; Férey, G. Role of Solvent-Host Interactions That Lead to Very Large Swelling of Hybrid Frameworks. *Science* **2007**, *315* (5820), 1828.

(13) Liu, Y.; Her, J.-H.; Dailly, A.; Ramirez-Cuesta, A. J.; Neumann, D. A.; Brown, C. M. Reversible Structural Transition in MIL-53 with Large Temperature Hysteresis. *J. Am. Chem. Soc.* **2008**, *130* (35), 11813-11818.

(14) Yot, P. G.; Ma, Q.; Haines, J.; Yang, Q.; Ghoufi, A.; Devic, T.; Serre, C.; Dmitriev, V.; Férey, G.; Zhong, C.; Maurin, G. Large breathing of the MOF MIL-47(VIV) under mechanical pressure: a joint experimental-modelling exploration. *Chem. Sci.* **2012**, *3* (4), 1100-1104.

(15) Demessence, A.; Long, J. R. Selective Gas Adsorption in the Flexible Metal-Organic Frameworks Cu(BDTri)L (L=DMF, DEF). *Chem. Eur. J.* **2010**, *16* (20), 5902-5908.

(16) Zhu, A. X.; Yang, Q. Y.; Kumar, A.; Crowley, C.; Mukherjee, S.; Chen, K. J.; Wang, S. Q.; D, O. N.; Shivanna, M.; Zaworotko, M. J. Coordination Network That Reversibly Switches between Two Nonporous Polymorphs and a High Surface Area Porous Phase. *J. Am. Chem. Soc.* **2018**, *140* (46), 15572-15576.

(17) Taylor, M. K.; Runcevski, T.; Oktawiec, J.; Bachman, J. E.; Siegelman, R. L.; Jiang, H.; Mason, J. A.; Tarver, J. D.; Long, J. R. Near-Perfect CO_2/CH_4 Selectivity Achieved through Reversible Guest Templating in the Flexible Metal-Organic Framework Co(bdp). *J. Am. Chem. Soc.* **2018**, *140* (32), 10324-10331.

(18) Lama, P.; Aggarwal, H.; Bezuidenhout, C. X.; Barbour, L. J. Giant Hysteretic Sorption of CO_2: *In Situ* Crystallographic Visualization of Guest Binding within a Breathing Framework at 298 K. *Angew. Chem. Int. Ed.* **2016**, *55* (42), 13271-13275.

(19) Gao, S.; Morris, C. G.; Lu, Z.; Yan, Y.; Godfrey, H. G. W.; Murray, C.; Tang, C. C.; Thomas, K. M.; Yang, S.; Schröder, M. Selective Hysteretic Sorption of Light Hydrocarbons in a Flexible Metal–Organic Framework Material. *Chem. Mater.* **2016**, *28* (7), 2331-2340.

(20) Nijem, N.; Wu, H.; Canepa, P.; Marti, A.; Balkus, K. J.; Thonhauser, T.; Li, J.; Chabal, Y. J. Tuning the Gate Opening Pressure of Metal–Organic Frameworks (MOFs) for the Selective Separation of Hydrocarbons. *J. Am. Chem. Soc.* **2012**, *134* (37), 15201-15204.

(21) Chen, B.; Liang, C.; Yang, J.; Contreras, D. S.; Clancy, Y. L.; Lobkovsky, E. B.; Yaghi, O. M.; Dai, S. A Microporous Metal–Organic Framework for Gas-Chromatographic Separation of Alkanes. *Angew. Chem. Int. Ed.* **2006**, *118* (9), 1418-1421.

(22) He, Y.; Xiang, S.; Chen, B. A microporous hydrogen-bonded organic framework for highly selective C_2H_2/C_2H_4 separation at ambient temperature. *J. Am. Chem. Soc.* **2011**, *133* (37), 14570-14573.

(23) Sen, S.; Hosono, N.; Zheng, J. J.; Kusaka, S.; Matsuda, R.; Sakaki, S.; Kitagawa, S. Cooperative Bond Scission in a Soft Porous Crystal Enables Discriminatory Gate Opening for Ethylene over Ethane. *J. Am. Chem. Soc.* **2017**, *139* (50), 18313-18321.

(24) Sheng, Y.; Chen, Q.; Yao, J.; Lu, Y.; Liu, H.; Dai, S. Guest-Induced Breathing Effect in a Flexible Molecular Crystal. *Angew. Chem. Int. Ed.* **2016**, *55* (10), 3378-3381.

(25) Atwood, J. L.; Barbour, L. J.; Jerga, A.; Schottel, B. L. Guest Transport in a Nonporous Organic Solid via Dynamic van der Waals Cooperativity. *Science* **2002**, *298* (5595), 1000.

(26) Allison, S.A.; Barrer, R.M. Sorption in the β-Phases of Transition-Metal(II) Tetra-(4-methylpyridine) Thiocyanates and Related Compounds. *J. Chem. Soc A* **1969**, 1717.

(27) Lin, R.-B.; He, Y.; Li, P.; Wang, H.; Zhou, W.; Chen, B. Multifunctional porous hydrogen-bonded organic framework materials. *Chem. Soc. Rev.* **2019**, *48* (5), 1362-1389.

(28) Venkataraman, D.; Lee, S.; Zhang, J.; Moore, J. S. An organic solid with wide channels based on hydrogen bonding between macrocycles. *Nature* **1994**, *371* (6498), 591-593.

(29) Nassimbeni, L. R., Physicochemical Aspects of Host–Guest Compounds. *Acc. Chem. Res.* **2003**, *36* (8), 631-637.

(30) McKeown, N. B. Nanoporous molecular crystals. *J. Mater. Chem.* **2010**, *20* (47), 10588-10597.

(31) Barbour, L. J. Crystal porosity and the burden of proof. *Chem. Commun.* **2006**, (11), 1163-1168.

(32) Jin, P.; Dalgarno, S. J.; Atwood, J. L., Mixed metal-organic nanocapsules. *Coordin. Chem. Rev.* **2010**, *254* (15-16), 1760-1768.

(33) Tozawa, T.; Jones, J. T. A.; Swamy, S. I.; Jiang, S.; Adams, D. J.; Shakespeare, S.; Clowes, R.; Bradshaw, D.; Hasell, T.; Chong, S. Y.; Tang, C.; Thompson, S.; Parker, J.; Trewin, A.; Bacsa, J.; Slawin, A. M. Z.; Steiner, A.; Cooper, A. I. Porous organic cages. *Nat. Mater.* **2009**, *8*, 973.

(34) Zhang, G.; Mastalerz, M. Organic cage compounds – from shape-persistency to function. *Chem. Soc. Rev.* **2014**, *43* (6), 1934-1947.

(35) Beuerle, F.; Gole, B. Covalent Organic Frameworks and Cage Compounds: Design and Applications of Polymeric and Discrete Organic Scaffolds. *Angew. Chem. Int. Ed.* **2018**, *57* (18), 4850-4878.

(36) Huang, S.-L.; Jin, G.-X.; Luo, H.-K.; Hor, T. S. A. Engineering Organic Macrocycles and Cages: Versatile Bonding Approaches. *Chem. Asian J.* **2015**, *10* (1), 24-42.

(37) Cooper, A. I. Porous Molecular Solids and Liquids. *ACS Cent. Sci.* **2017**, *3* (6), 544-553.

(38) Mitra, T.; Wu, X.; Clowes, R.; Jones, J. T.; Jelfs, K. E.; Adams, D. J.; Trewin, A.; Bacsa, J.; Steiner, A.; Cooper, A. I. A soft porous organic cage crystal with complex gas sorption behavior. *Chem. Eur. J.* **2011**, *17* (37), 10235-10240.

(39) Zhang, C.; Wang, Q.; Long, H.; Zhang, W. A Highly C70 Selective Shape-Persistent Rectangular Prism Constructed through One-Step Alkyne Metathesis. *J. Am. Chem. Soc.* **2011**, *133* (51), 20995-21001.

(40) Bera, S.; Basu, A.; Tothadi, S.; Garai, B.; Banerjee, S.; Vanka, K.; Banerjee, R. Odd–Even Alternation in Tautomeric Porous Organic Cages with Exceptional Chemical Stability. *Angew. Chem. Int.. Ed.* 2**017**, *56* (8), 2123-2126.

(41) Lee, S.; Yang, A.; Moneypenny, T. P.; Moore, J. S. Kinetically Trapped Tetrahedral Cages via Alkyne Metathesis. *J. Am. Chem. Soc.* **2016**, *138* (7), 2182-2185.

(42) Hong, S.; Rohman, M. R.; Jia, J.; Kim, Y.; Moon, D.; Kim, Y.; Ko, Y. H.; Lee, E.; Kim, K. Porphyrin Boxes: Rationally Designed Porous Organic Cages. *Angew. Chem. Int. Ed.* **2015**, *54* (45), 13241-13244.

(43) Avellaneda, A.; Valente, P.; Burgun, A.; Evans, J. D.; Markwell-Heys, A. W.; Rankine, D.; Nielsen, D. J.; Hill, M. R.; Sumby, C. J.; Doonan, C. J. Kinetically Controlled Porosity in a Robust Organic Cage Material. *Angew. Chem. Int. Ed.* **2013**, *52* (13), 3746-3749.

(44) Ding, H.; Yang, Y.; Li, B.; Pan, F.; Zhu, G.; Zeller, M.; Yuan, D.; Wang, C. Targeted synthesis of a large triazine-based [4+6] organic molecular cage: structure, porosity and gas separation. *Chem. Commun.* **2015**, *51* (10), 1976-1979.

(45) Greenaway, R. L.; Holden, D.; Eden, E. G. B.; Stephenson, A.; Yong, C. W.; Bennison, M. J.; Hasell, T.; Briggs, M. E.; James, S. L.; Cooper, A. I. Understanding gas capacity, guest selectivity, and diffusion in porous liquids. *Chem. Sci.* **2017**, *8* (4), 2640-2651.

(46) Henke, S.; Schneemann, A.; Wutscher, A.; Fischer, R. A. Directing the breathing behavior of pillared-layered metal-organic frameworks via a systematic library of functionalized linkers bearing flexible substituents. *J. Am. Chem. Soc.* **2012**, *134* (22), 9464-9474.

(47) Yamazaki, T.; Takahashi, Y.; Yoshida, D. Adsorption of several gases on flexible metal organic framework [Cu(dhbc)2(4,4′-bpy)]·H_2O. *J. Colloid Interface Sci.* **2011**, *362* (2), 463-469.

(48) Yang, Q.Y.; Lama, P.; Sen, S.; Lusi, M.; Chen, K.J.; Gao, W.Y.; Shivanna, M.; Pham, T.; Hosono, N.; Kusaka, S.; Perry, J.J.; Ma, S.; Space, B.; Barbour, L.J.; Kitagawa, S.; Zaworotko, M.J. Reversible Switching between Highly Porous and Nonporous Phases of an Interpenetrated Diamondoid Coordination Network that Exhibits Gate-Opening at Methane Storage Pressures. *Angew. Chem. Int. Ed.* **2018**, *57* (20), 5684-5689.

(49) Li, L.; Wen, H. M.; He, C.; Lin, R. B.; Krishna, R.; Wu, H.; Zhou, W.; Li, J.; Li, B.; Chen, B., A Metal-Organic Framework with Suitable Pore Size and Specific Functional Sites for the Removal of Trace Propyne from Propylene. *Angew. Chem. Int. Ed.* **2018**, *57* (46), 15183-15188.

(50) Li, L.; Krishna, R.; Wang, Y.; Yang, J.; Wang, X.; Li, J., Exploiting the gate opening effect in a flexible MOF for selective adsorption of propyne from C1/C2/C3 hydrocarbons. *J. Mater. Chem. A* **2016**, *4* (3), 751-755.

Insert Table of Contents artwork here